**UNIVERSIDAD NACIONAL AUTÓNOMA DE MÉXICO**

**FACULTAD DE QUÍMICA**

*MODELACIÓN DE POLIMERIZACIÓN RAFT DE MMA EN DIÓXIDO DE CARBONO SUPERCRÍTICO USANDO LA ECUACIÓN DE ESTADO PC-SAFT*

**ACTIVIDAD DE INVESTIGACIÓN**

**QUE PARA OBTENER EL TÍTULO DE:**

**INGENIERO QUÍMICO**

**PRESENTA:**

**JESÚS EDUARDO RIVERA PELÁEZ**

**CDMX          2022**

**JURADO ASIGNADO:**

PRESIDENTE:      M en I. Fernando Morales Morales

VOCAL:           Dr. Milton García Medeiros De Oliveira

SECRETARIO:      Dr. Porfirio López Domínguez

1er. SUPLENTE:   M en I. Leticia Valle Arizmendi

2° SUPLENTE:     Dr. Alberto Rosas Aburto

**SITIO DONDE SE DESARROLLÓ EL TEMA:**

FACULTAD DE QUÍMICA, DEPARTAMENTO DE INGENIERÍA QUÍMICA, CONJUNTO E, CIUDAD UNIVERSITARIA.

**ASESOR DEL TEMA:**

Dr. Porfirio López Domínguez

_____

**SUSTENTANTE:**

Jesús Eduardo Rivera Peláez

_____

# Contenido

AGRADECIMIENTOS

**PROTOCOLO DE INVESTIGACIÓN**

TEMA

Modelación de polimerización RAFT de MMA en dióxido de carbono supercrítico usando la ecuación de estado PC-SAFT.

INTRODUCCIÓN

La necesidad de reducir las emisiones de disolventes orgánicos a la atmosfera en las síntesis poliméricas tradicionales ha llevado a la búsqueda de disolventes alternativos como medio de reacción. Algunos disolventes que han recibido mucha atención son: el dióxido de carbono supercrítico ($scCO_2$), agua, líquidos iónicos y polietilenglicol. En particular, el uso de estos disolventes ha aumentado en el campo de la polimerización radical por desactivación reversible (RDRP´s, por sus siglas en inglés *reversible deactivation radical polymerization*). Los sistemas RDRP´s más estudiados durante los últimos 30 años son la polimerización por transferencia de cadena de adición-fragmentación reversible (RAFT), polimerización radicálica por transferencia de átomo (ATRP) y la polimerización radicálica mediada por nitróxidos (NMP). La razón del uso de sistemas RDRP´s como método de polimerización es debido a que se han llevado a cabo polimerizaciones exitosas en condiciones homogéneas y heterogéneas, desarrollando polímeros con microestructuras controladas los cuales pueden ser útiles en diferentes campos de la industria y la investigación.

Actualmente, $scCO_2$ es atractivo como medio de reacción debido a que el producto se recupera simplemente descargando el $CO_2$ del reactor. Generalmente, las reacciones en $scCO_2$ ocurren como procesos heterogéneos debido a la nula solubilidad de polímeros de alta masa molar en el solvente. Sin embargo, los procesos poliméricos heterogéneos conllevan a un desafío común en la química el cual es el estudio de la transferencia de masa entre las diferentes fases y especies poliméricas involucradas. También es importante señalar que los datos

experimentales son difíciles de obtener debido a que los reactores trabajan a presiones tan altas como 500 bar.

Anteriormente se han utilizado ecuaciones semi-empiricas para la partición de solvente y monómero entre las diferentes fases presentes, así como el uso de software comercial para la partición de componentes de bajo peso molecular entre las fases de la mezcla de reacción. En la presente investigación se aplica la ecuación de estado PC-SAFT para describir la partición de las especies entre las fases presentes, así como se comparan los resultados con datos experimentales reportados en la literatura. Se analizará el efecto de la presión y la temperatura en la polimerización del metacrilato de metilo (MMA).

OBJETIVOS DE LA INVESTIGACIÓN

El objetivo de esta contribución es modelar y describir la polimerización RAFT del metacrilato de metilo en dióxido de carbono supercrítico usando la ecuación de estado PC-SAFT.

OBJETIVOS PARTICULARES

1. Desarrollar tres modelos matemáticos (Modelos A, B y C) para modelar la polimerización del metacrilato de metilo y compararlos entre sí.

2. Utilizar el método de los momentos para simplificar el balance de materia en ciertos modelos desarrollados.

3. Modelar la polimerización del metacrilato de metilo utilizando un software comercial.

4. Comparar los resultados de las modelaciones de los tres modelos desarrollados con resultados experimentales encontrados en la literatura

5. Estimar los parámetros de interacción binaria a partir de datos experimentales encontrados en la literatura para el sistema de polimerización estudiada.

6. Describir el efecto de la presión y la temperatura sobre la polimerización del metacrilato de metilo utilizando los tres modelos desarrollados.

## MATERIALES Y MÉTODOS

Para los modelos matemáticos A y C, se obtuvieron las ecuaciones diferenciales correspondientes a los balances de materia para cada componente. Se usó el lenguaje de programación Fortran y se resolvieron usando compiladores Intel en la supercomputadora Miztli (UNAM, México). En el caso del Modelo B, se usó el software comercial Predici® en una computadora de escritorio. Los parámetros de interacción binaria fueron estimados usando Aspen Plus V8.8 y VLXE.

## DISEÑO EXPERIMENTAL

Se desarrollarán tres modelos para explicar la polimerización RAFT del MMA. En el modelo A se usarán ecuaciones de partición semi-empiricas para explicar la transferencia de masa de las especies entre la fase dispersa y continua. Se usará el método de los momentos para simplificar el balance de materia.

En el modelo A se considerarán tres etapas durante la reacción; etapa 1 donde la reacción inicia y las especies se encuentran en una sola fase (reacción homogénea) hasta una conversión crítica ($x_{sa}$) en el que se presenta una segunda fase; en la etapa 2 hay presentes dos fases y la polimerización ocurre en ambas fases; en la etapa 3 la polimerización ocurre solamente en la fase dispersa.

El modelo B utiliza el software comercial Predici® implementando ecuaciones de transferencia con la finalidad de describir la transferencia de masa de las especies de baja masa molecular y los radicales activos entre las fases continuas y dispersa.

El modelo C usará la ecuación de estado PC-SAFT para describir el equilibrio L-L y de igual manera que el modelo A usará el método de momentos para simplificar el balance de materia. Similar al modelo A, existe una conversión crítica $x_{sa}$ en el que los oligómeros ya no son solubles en la fase continua y se presentan dos fases por lo que la reacción se lleva a cabo en ambas fases.

REVISIÓN BIBLIOGRÁFICA PRELIMINAR DEL TEMA

1. López-Domínguez, P., Jaramillo-Soto, G., & Vivaldo-Lima, E. (2018). "A modeling study on the RAFT polymerization of vinyl monomers in supercritical carbon dioxide", Recuperado de *Macromolecular Reaction Engineering*, 12(4).

2. López-Domínguez, P., Hernández-Ortiz, J. C., & Vivaldo-Lima, E. (2018). "Modeling of RAFT copolymerization with crosslinking of Styrene/Divinylbenzene in supercritical carbon dioxide", Recuperado de *Macromolecular Theory and Simulations*, 27, 1700064.

3. Porfirio López-Domínguez, Gabriel Jaramillo Soto, Eduardo Vivaldo-Lima. (2018). "A Modeling Study on the RAFT Polymerization of Vinyl Monomers in Supercritical Carbon Dioxide", Recuperado de *Macromolecular Reaction Engineering,* 12, 1800011.

4. Michael Görnert and Gabriele Sadowski. (2018). "Phase-equilibrium measurement and modeling of the PMMA/MMA/carbon dioxide ternary system". Recuperado de *Journal of Supercritical Fluids,* 46, 218-225

5. Samira Masoumi, Thomas A. Duever, Alexander Penlidis, Reza Azimi, Porfirio López-Domínguez, Eduardo Vivaldo-Lima. (2018). "Model Discrimination between RAFT Polymerization Models Using Sequential Bayesian Methodology", Recuperado de *Macromolecular Theory and Simulations,* 27(5), 1800016.

6. Porfirio López-Domínguez, Diego Alberto Clemente-Montes, Eduardo Vivaldo-Lima*, (2020). "Modeling of reversible deactivation radical polymerization of vinyl monomers promoted by redox initiation using NHPI and xanthone", Recuperado de *Macromolecular Reaction Engineering.*

7. Rubén Cuatepotzo-Díaz, Brenda Larisa López-Méndez, Porfirio López-Domínguez, Martha Eugenia Albores-Velasco, Alexander Penlidis, and

Eduardo Vivaldo-Lima*. (2020). "The Role of Nitroxide Degradation on the Efficiency of the Controller in Nitroxide-Mediated Radical Polymerization (NMP) of Styrene", Recuperado de *Ind. Eng. Chem.* Res. 2020, 59, 40, 17786–17795.

8. Gabriel Jaramillo-Soto, M. Luz Castellanos-Cárdenas, Pedro R. García-Morán, Eduardo Vivaldo-Lima*, Gabriel Luna-Bárcenas, and Alexander Penlidis. (2008). "Simulation of Reversible Addition-Fragmentation Chain Transfer (RAFT) Dispersion Polymerization in Supercritical Carbon Dioxide", Recuperado de *Macromolecular Theory and Simulations*, 17, 280-289.

9. Pedro R. García-Morán, Gabriel Jaramillo-Soto, Martha E. Albores-Velasco and Eduardo Vivaldo-Lima*. (2009). "An Experimental Study on the Free-Radical Copolymerization Kinetics with Crosslinking of Styrene and Divinylbenzene in Supercritical Carbon Dioxide", Recuperado de *Macromolecular Reaction Engineering*, 3(1), 58-70.

**ARTÍCULO**

# MODELING OF RAFT POLYMERIZATION OF MMA IN SUPERCRITICAL CARBON DIOXIDE USING THE PC-SAFT EQUATION OF STATE[1]

Porfirio López-Domínguez[a], Jesús Eduardo Rivera-Peláez[a], Gabriel Jaramillo-Soto[a],

José Fernando Barragán-Aroche[a] and Eduardo Vivaldo-Lima[ab]

ABSTRACT

The kinetics and evolution of molar mass averages for reversible addition-fragmentation chain transfer (RAFT) dispersion polymerization of vinyl monomers in supercritical carbon dioxide ($scCO_2$) is addressed using three mathematical models (models A, B and C). Models A and C are based on the methods of moments. The partition of components is calculated using simple partition equations in model A, whereas the perturbed-chain statical associating fluid theory (PC-SAFT) equation of state is employed in model C. On the other hand, in model B, the polymerization scheme and mass transport of the species among the present phases are calculated by using the Predici® commercial software. The PC-SAFT equation of state is also used to calculate the solubility of oligomers in the reaction mixture. The calculated profiles of monomer conversion versus time and molar mass averages versus

[a] *Facultad de química, Departamento de Ingeniería Química, Universidad Nacional autónoma de México, 04510, Ciudad de México, México. E-mail:* [vivaldo@unam.mx](mailto:vivaldo@unam.mx)

[b] *Institute for polymer Research, Department of Chemical Engineering, University of Waterloo, Waterloo, Ontario, Canada*

conversion are compared with available experimental data for dispersion polymerization of methyl methacrylate (MMA) in scCO$_2$, using 2,2´-azobis(2-methylpropionitrile) (AIBN) and s-thiobenzoyl thioglycolic acid (TBTGA) as initiator and controller, respectively. The effects of temperature and pressure are also analyzed.

INTRODUCTION

During the last two decades, reversible deactivation radical polymerizations (RDRPs) have been successfully conducted in homogeneous and heterogeneous conditions yielding polymers with controlled microstructures for a diverse range of applications.[1,2] The most studied RDRP systems are reversible addition-fragmentation chain transfer (RAFT) polymerization,[3,4] atom transfer radical polymerization (ATRP),[5,6] and nitroxide-mediated radical polymerization (NMP).[7,8] There has been an increasing interest on the study of RDRPs conducted in "green solvents", such as water, supercritical CO$_2$ (scCO$_2$), ionic liquids, and low molar mass poly(ethylene glycol)s.[9,10]Recently, well-defined poly-(dodecafluoroheptyl methacrylate)-*b*-poly(methyl methacrylate) (PDFMA-*b*-PMMA) using AIBN and 1-docecyl*S*´-(α-α´-dimethyl-α´´-acetic acid) trithiocarbonate (DDMAT) was synthesized in scCO$_2$ at 70 °C and 300 bar. [11] Scanning electron microscopy (SEM) images showed that nanoparticles with an average size of 425 nm and with narrow size distributions were obtained. Jennings *et al.*[12] reported the one-pot synthesis of poly(benzyl methacrylate (BzMA)-*b*-PMMA) and PMMA-*b*-polystyrene(PS) using AIBN/DDMAT/scCO$_2$ at 65 °C and 275 bar. It was found that the block control

capacity of the process was excellent when initiator content and targeted number average chain lengths ($\bar{P}_n$) where both decreased.[12]

Most polymerizations carried out in scCO$_2$, proceed as dispersion as dispersion polymerization processes. At the star of polymerization in scCO$_2$, the monomer and CO$_2$ form a homogeneous phase. The first propagation steps yield small oligomer molecules which are also expected to be soluble in the reaction medium until they reach a critical chain-length and then phase separate. Dispersion polymerization is a type of precipitation polymerization.[13,14] The low or null solubility of high-molar-mass macromolecules in scCO$_2$ leads to two reaction loci: the CO$_2$-rich and the polymer-rich phases. Three approaches have been used in the literature to account for the partition of monomer and CO$_2$ in such phases: (a) application of the Sanchez-Lacombe equation of state (SL-EoS)[15-18] for calculation of the phase equilibrium and mass transfer of low molar mass species; (b) assuming mass transfer of low molar mass species and polymer radicals between continuous and dispersed phases using the "phase-exchange" and "*k(s)*-termination" steps of the Predici® software,[19,20] and (c) use of semi-empirical partition coefficient[21-25] for calculation of phase equilibrium and mass transfer of polymer species.

**Table 1**    Polymerization scheme for RAFT homopolymerization of vinyl monomers in phase $\Psi$

| Reaction | Representation | Kinetic Coefficient |
|---|---|---|
| Initiation | $I_\Psi \rightarrow 2R_{in,\Psi}$ | $f_\Psi, k_{d,\Psi}$ |
| First propagation | $R_{in,\Psi} + M_\Psi \rightarrow R_\Psi(1)$ | $k_{p,\Psi}$ |
| Propagation | $R_\Psi(S) + M_\Psi \rightarrow R_\Psi(s+1)$ | $k_{p,\Psi}$ |
| Termination by combination and disproportion | $R_\Psi(S) + R_\Psi(r) \rightarrow P_\Psi(s+r)$ | $k_{tc,\Psi}$ |
|  | $R_\Psi(S) + R_\Psi(r) \rightarrow P_\Psi(s) + P_\Psi(r)$ | $k_{td,\Psi}$ |
| Reversible chain transfer to RAFT agent | $R_\Psi(S) + AB_\Psi \leftrightarrow R_\Psi(s)AB \leftrightarrow PA_\Psi(s) + B_{\dot\Psi}$ | $k_{add,\Psi}, k_{bd,\Psi}$ |
| Main equilibrium | $R_\Psi(S) + PA_\Psi(r) \leftrightarrow R(s)AR_\Psi(r)$ | $k_{a,\Psi}, k_{b,\Psi}$ |
|  | $\leftrightarrow PA_\Psi(s) + R_\Psi(r)$ |  |
| Intermediate radical termination | $R_\Psi(S) + R(r)AR_\Psi(l) \rightarrow T_\Psi(s+r+l)$ | $k_{tir,\Psi}$ |

**Table 2**  Definition of moments for the different polymer distributions in phase $\Psi$

| Distribution | Moment definition | Equation |
|---|:---:|:---:|
| Living polymer | $$Y_{m.\Psi} = \sum_{s=1}^{\infty} s^m [R_\Psi(s)]$$ | (1) |
| Dormant polymer | $$Z_{m.\Psi} = \sum_{s=1}^{\infty} s^m [PA_\Psi(s)]$$ | (2) |
| Dead polymer | $$Q_{m.\Psi} = \sum_{s=1}^{\infty} s^m [P_\Psi(s)]$$ | (3) |
| One-arm adduct | $$E_{m.\Psi} = \sum_{s=1}^{\infty} s^m [R_\Psi(s)AB]$$ | (4) |
| Two-arms adduct | $$F_{mn.\Psi} = \sum_{r=1}^{\infty}\sum_{s=1}^{\infty} r^m s^n [R(s)AR_\Psi(r)]$$ | (5) |
| Three-arms adduct | $$G_{mnu.\Psi} = \sum_{l=1}^{\infty}\sum_{r=1}^{\infty}\sum_{s=1}^{\infty} s^m r^n l^u [T_\Psi(s+r+l)]$$ | (6) |

**Table 3**  Material balance equations for low molas mass species in phase $\Psi$

| Species | Material balance | Equation |
|---|:---:|:---:|
| Initiator | $$\frac{1}{V_\Psi}\frac{d(V_\Psi[I_\Psi])}{dt} = -k_{d,\Psi}[I_\Psi]$$ | (7) |
| Monomer | $$\frac{1}{V_\Psi}\frac{d(V_\Psi[M_\Psi])}{dt} = -k_{p,\Psi}[M_\Psi]\left([R_{in,\Psi}] + Y_{0,\Psi}\right)$$ | (8) |
| Primary free radicals | $$\frac{1}{V_\Psi}\frac{d(V_\Psi[R_{in,\Psi}])}{dt} = 2f_\Psi k_{d,\Psi}[I_\Psi] - k_{p,\Psi}[M_\Psi][R_{in,\Psi}]$$ | (9) |
| RAFT agent | $$\frac{1}{V_\Psi}\frac{d(V_\Psi[AB_\Psi])}{dt} = -k_{add,\Psi}[AB_\Psi]Y_{0,\Psi} + k_{\_add,\Psi}E_{0,\Psi}$$ | (10) |
| RAFT agent leaving group | $$\frac{1}{V_\Psi}\frac{d(V_\Psi[B_\Psi])}{dt} = k_{bd,\Psi}E_{0,\Psi} - k_{bd,\Psi}Z_{0,\Psi}[B_\Psi] \\ - k_{p,\Psi}[M_\Psi][B_\Psi]$$ | (11) |

The influence of temperature and pressure on the performance and properties of polymer/supercritical-fluid systems has been successfully modeled with the use of cubic equations of state (or its variants), and also using the so-called lattice-fluid theory and statistical associating fluid theory (SAFT).[26] One of the modifications of SAFT, namely, perturbed chain statistical associating fluid theory (PC-SAFT) has shown to quantitatively describe cloud points of homopolymer and copolymer mixtures.[27-29] Görnet an Sadowski[30] calculated concentration profiles for the polymer-rich phase of a PMMA/MMA/$CO_2$ system using experimental data obtained by cloud point and infrared (IR) spectra measurements. The effects of temperature, pressure and polymer molar mass on process performance and material properties were nicely described with a mathematical model based on PC-SAFT.[30]

Herein, three approaches for the analysis of RAFT polymerization of MMA in scCO$_2$ are compared: model A, based upon semi-empirical partition equations and the method of moments; in model B, transfer equations are implemented in Predici®; and in model C, the liquid-liquid (LL) equilibrium is calculated using the PC-SAFT equation of state (EoS), coupled with the method of moments. In the latter model, it is assumed that the oligomers are monodisperse and that their chain-length increases linearly with conversion, if an appropriate RAFT agent is used.[31,32] Models A and B have already been used to model this type of polymerization.[19-25] They are used here to validate model C, which had not been used earlier for the modelling of these polymerizations.

Experimental data of MMA conversion *versus* time and molar mass development at several temperatures (65-85 °C) and pressures (100-500 bar) for polymerizations carried out in scCO$_2$ were used to validate the model.[33]

17

**Table 4** Moment equations for polymer distributions in RAFT polymerizations of vinyl monomers, in phase $\Psi$

| Species | Material balance | Equation |
|---|---|---|
| Living polymer | $$\frac{1}{V_\Psi}\frac{d(V_\Psi Y_{m,\Psi})}{dt} = k_{p,\Psi}[M_\Psi]\left([R_{in,\Psi}] + [B_\Psi] + \sum_{s=0}^{m}\binom{m}{s}Y_{s,\Psi} - Y_{m,\Psi}\right)$$ $$- k_{t,\Psi}Y_{m,\Psi}Y_{0,\Psi} - k_{tir,\Psi}Y_{m,\Psi}F_{00,\Psi} - k_{add,\Psi}Y_{m,\Psi}[AB_\Psi]$$ $$+ k_{\_add,\Psi}E_{m,\Psi} - (k_{a,\Psi} + k_{\_b,\Psi})Y_{m,\Psi}Z_{0,\Psi} + (k_{\_a,\Psi}$$ $$+ k_{b,\Psi})F_{m0,\Psi} - k_{transferA,\Psi}\left(Y_{m,\Psi} - \frac{Y_{m,\Psi2}}{\zeta_p}\right)$$ | (12) |
| Dormant polymer | $$\frac{1}{V_\Psi}\frac{d(V_\Psi Z_{m,\Psi})}{dt} = k_{bd}E_m - k_{\_bd}Z_m B_\Psi - (k_{a,\Psi} + k_{\_b,\Psi})Z_{m,\Psi}Y_{0,\Psi} + (k_{\_a,\Psi}$$ $$+ k_{b,\Psi})F_{m0,\Psi} - k_{transferA,\Psi}\left(Z_{m,\Psi} - \frac{Z_{m,\Psi2}}{\zeta_p}\right)$$ | (13) |
| Dead polymer | $$\frac{1}{V_\Psi}\frac{d(V_\Psi Q_{m,\Psi})}{dt} = \frac{1}{2}k_{tc,\Psi}\sum_{s=0}^{m}\binom{m}{s}Y_{s,\Psi}Y_{m-s,\Psi} + k_{td,\Psi}Y_{m,\Psi}Y_{0,\Psi}$$ | (14) |
| One-arm adduct | $$\frac{1}{V_\Psi}\frac{d(V_\Psi E_{m,\Psi})}{dt} = k_{add,\Psi}Y_{m,\Psi}[AB_\Psi] - (k_{\_add,\Psi} + k_{bd,\Psi})E_{m,\Psi}$$ $$+ k_{\_bd}Z_m[B_\Psi]$$ | (15) |
| Two-arms adduct | $$\frac{1}{V_\Psi}\frac{d(V_\Psi F_{mn,\Psi})}{dt}$$ $$= (k_{a,\Psi} + k_{\_b,\Psi})Y_{m,\Psi}Z_{n,\Psi} - 2(k_{\_a,\Psi} + k_{b,\Psi})F_{mn,\Psi} + (k_{a,\Psi}$$ $$+ k_{\_b,\Psi})Z_{m,\Psi}Y_{n,\Psi} - k_{tir,\Psi}F_{mn,\Psi}Y_{0,\Psi}$$ $$- k_{transferA,\Psi}\left(F_{mn,\Psi} - \frac{F_{mn,\Psi2}}{\zeta_P}\right)$$ | (16) |

| Three-arms adduct | $\dfrac{1}{V_\Psi}\dfrac{d(V_\Psi G_{mnu,\Psi})}{dt} = k_{tir,\Psi}F_{mn,\Psi}Y_{u,\Psi}$ | (17) |

MODELING

The polymerization scheme, kinetic and moment equations summarized in Tables 1-5 (eqn (1)-(17)) are very similar to the ones considered in our previous study[20] for the polymerization of styrene in scCO$_2$. As stated earlier, the key change here, and the focus of this contribution, is the use of the PC-SAFT EoS for calculation of the partition of components between the continuous and dispersed phases.

The RAFT polymerization of vinyl monomers involves, on the one hand, conventional reactions such as generation of primary radicals, $R_{in,\psi}$, from initiator, $I_\psi$, first propagation with monomers molecules, $M_\psi$, propagation and termination by both combination and disproportionation of active radicals, $R_\psi(s)$, in phase Ψ (Ψ = con (dis) for continuous (dispersed) phase), as summarized in Table 1. On the other hand, the RAFT agent, $AB_\psi$, reacts with the active radicals to form one-arm adduct, $R_\psi(s)$AB, which in turn fragments into dormant polymer (macro-RAFT agent, $PA_\psi(s)$), and leaving free radical $B_\psi$. The main equilibrium represents a reversible reaction between active radicals and macro-RAFT agent (dormant polymer) to yield two-arm adduct, $R(s)AR_\psi(r)$.

Although there are simpler models than one used here for RAFT polymerization where no intermediate two-arm adduct is produced or where addition and fragmentation steps are not reversible, the polymerization scheme shown in

Table 1 not only describes the chemical route originally proposed by the people from CSIRO,[35] but it has been shown to better represent RAFT polymerization systems in a wide range of polymerization conditions.[35]

Intermediate radical termination between two-arm adduct and active radicals producing three-arm dead polymer ($T_\Psi(s + r + l)$) was also considered.

Once formed, polymer species $P_\Psi(s)$ and $T_\Psi(s)$ do not undergo further reaction and only contribute to global molar masses. On the other hand, the main equilibrium between $R(s)$, $R(s)AR_\Psi(r)$ and $PA_\Psi(s)$ can be affected by migration of those species from the continuous to the dispersed phase, and *vice versa*. Mass transfer of polymer species of size $s$, $Pol_\Psi(s)$, from phase $\Psi$ to phase $\Psi_2$ (second phase) is modeled using a simple mass transfer rate expression, given by eqn (18) and (19) in models A and C, where $\zeta_P(s)$ is partition coefficients for polymer species of size $s$, or Predici´s $k(s)$-termination step in model B. The full molar mass distribution is required to account for chain length-dependent mass transport parameters, as reported for the case of conventional radical polymerization of MMA.[15]

$$\frac{dPol_\Psi(s)}{V_\Psi dt} = -k_{transferA,\Psi}(s)\left([Pol_\Psi(s)] - \frac{[Pol_{\Psi_2}(s)]}{\zeta_P(s)}\right) \qquad (18)$$

$$\frac{dPol_\Psi(s)}{V_\Psi dt} = -k_{transferB,\Psi}(s)([Pol_\Psi(s)]) \qquad (19)$$

**Table 5**    Steps used in Predici® for RAFT dispersion polymerization of vinyl monomers

| Reaction | Step name | Step pattern | Kinetic |
|---|---|---|---|
| Initiation and first propagation | Initiation (rad) | $I \rightarrow 2I^*$ | $f_\Psi, k_{d,\Psi}$ |
| | | $I^* + M \rightarrow R(1)$ | $k_{p,\Psi}$ |
| Propagation | Propagation | $R(s) + M \rightarrow R(s+1)$ | $k_{p,\Psi}$ |
| Irreversible chain transfer to | Change | $R(s) + AB \rightarrow RAB(s)$ | $k_{add,\Psi}$ |
| | Change | $RAB(s) \rightarrow PA(s) + B^*$ | $k_{bd,\Psi}$ |
| Addition | D-Termination | $R(s) + PA(r) \rightarrow Q(s)$ | $k_{a,\Psi}$ |
| Fragmentation | Change | $Q(s) \rightarrow PA(s)$ | $k_{b,\Psi}$ |
| | | $S(s) \rightarrow R(s)$ | $k_{b,\Psi}$ |
| Intermediate radical termination | Condensation | $R(s) + Q(r) \rightarrow T(s+r)$ | $k_{tir,\Psi}$ |
| | | $R(s) + S(r) \rightarrow T(s+r)$ | $k_{tir,\Psi}$ |
| Termination | Termination by | $R(s) + R(r) \rightarrow P(s+r)$ | $k_{tc,\Psi}$ |
| | combination/disproportion | $R(s) + R(r) \rightarrow P(s)$ | $k_{td,\Psi}$ |
| Phase transfer of LMS | Phase exchange | $LMS_{con} \leftrightarrow LMS_{dis}$ | $k_{pe}$ |
| Active radical transfer | $k(s)$-Termination | $R_{con}(s) \leftrightarrow LMS_{dis}(s)$ | $k_{transferB,\Psi}$ |

**The method of moments (MMs) applied to RAFT polymerization**

The method of moments is an efficient approach for the calculation of average polymer properties, especially in the modelling of structurally linear polymerizations, such as number-average chain length, $\bar{P}_n$, and dispersity of molar mass, Đ. In the present study, the definition of moments for the different polymer distributions in phase Ψ are summarized in Table 2 (eqn (1)-(6)). The rate of consumption of low

molar mass species and polymer populations are listed in Tables 3 and 4 (eqn (7)-(17)), respectively.

It was assumed for simplification purposes that mass transport coefficient, $k_{transfer\,A}$, and polymer partition coefficient, $\zeta_P$, remain constant throughout the polymerization.

Global number and weight-average chain lengths ($\bar{P}_n$, $\bar{P}_w$) are calculated according to eqn (20)-(25). It should be noted that global variables are represented without subscript Ψ. Global values for concentrations of low molar mass species and polymer molecules are given by the sum if their respective values in each phase (*e.g.*, $M = \sum_\Psi [M]_\Psi V_\Psi$ and $Y_0 = \sum_\Psi Y_{0,\Psi} V_0$). Dispersity of molar mass, Đ, is defined as the ratio of $\bar{P}_w$ to $\bar{P}_n$ (see eqn (25)).

$$\mu_{0,\Psi} = Y_{0,\Psi} + Z_{0,\Psi} + Q_{0,\Psi} + S_{0,\Psi} + E_{0,\Psi} + \frac{1}{2}F_{00,\Psi} + \frac{2}{3}G_{000,\Psi} \tag{20}$$

$$\mu_{1,\Psi} = Y_{1,\Psi} + Z_{1,\Psi} + Q_{1,\Psi} + E_{1,\Psi} + \frac{1}{2}\left(F_{10,\Psi} + F_{01,\Psi}\right)$$

$$+ \frac{2}{3}\left(G_{100,\Psi} + G_{010,\Psi} + G_{001,\Psi}\right) \tag{21}$$

$$\mu_{2,\Psi} = Y_{2,\Psi} + Z_{2,\Psi} + Q_{2,\Psi} + E_{2,\Psi} + \frac{1}{2}\left(F_{20,\Psi} + F_{02,\Psi} + 2F_{11,\Psi}\right) + \frac{2}{3}\left(G_{200,\Psi} + G_{020,\Psi} + G_{002,\Psi} + 2\left(G_{110,\Psi} + G_{101,\Psi} + G_{011,\Psi}\right)\right) \tag{22}$$

$$\bar{P}_n = \frac{\mu_{1,con}V_{con} + \mu_{1,dis}V_{dis}}{\mu_{0,con}V_{con} + \mu_{1,dis}V_{dis}} \tag{23}$$

$$\bar{P}_w = \frac{\mu_{2,con}V_{con} + \mu_{2,dis}V_{dis}}{\mu_{1,con}V_{con} + \mu_{1,dis}V_{dis}} \tag{24}$$

$$Đ = \frac{\bar{P}_w}{\bar{P}_n} \tag{25}$$

**Model A: simple partition of components.** The modeling of dispersion polymerization of vinyl monomers has been studied with the use of a simple model for the partition of monomer and solvent, coupled with the method of moments, and

considering a three-stage polymerization in terms of monomer conversion.[36] Such approach has been successfully applied to conventional free radical (co)polymerization[21-24] and recently, a modified version of it was applied to RAFT (co)polymerizations.[20-25].

Stage 1 ($0 \leq x < x_{sa}$). The reaction begins as a homogeneous reaction until a limiting monomer conversion, $x_{sa}$, is reached. The amount of monomer in each phase is calculated using eqn (26) and (27).

$$M_{con} = M_0(1 - x) \tag{26}$$

$$M_{dis} = 0 \tag{27}$$

Stage 2 ($x_{sa} \leq x < x_c$). It is assumed that two phases, polymer-rich and $CO_2$ rich phases, are present. The amount of monomer in each phase is calculated using eqn (28) and (29), where $K_s$ is defined as the mass ratio of $CO_2$ to monomer in the monomer in the dispersed phase.

$$M_{con} = M_0\left(1 - x - \frac{x\left(\frac{1}{x_c}-1\right)}{1+K_s}\right) \tag{28}$$

$$M_{dis} = M_0\left(\frac{x\left(\frac{1}{x_c}-1\right)}{1+K_s}\right) \tag{29}$$

Stage 3 ($x_c \leq x < 1$). In this stage, polymerization occurs only in the dispersed phase as defined by eqn (30) and (31).

$$M_{con} = 0 \tag{30}$$

$$M_{dis} = M_0(1 - x) \tag{31}$$

As summary, parameters $x_{sa}$, $x_c$, and $K_s$ are to be estimated for each polymerization case and their values lead to low or high monomer concentrations attained in the dispersed phase.

Regarding the partition of initiator used in models A and C, it was assumed that the ratio of initiator to total monomer is the same in both phases, leading to eqn (32) and (33) for the amount of initiator in both phases.[20,23-25] Similar relationships were assumed for RAFT agent, resulting in eqn (34) and (35).

$$I_{con} = \frac{I}{1 + \frac{M_{dis}}{M_{con}}} \tag{32}$$

$$I_{dis} = I - I_{con} \tag{33}$$

$$AB_{con} = \frac{AB}{1 + \frac{M_{dis}}{M_{con}}} \tag{34}$$

$$AB_{dis} = AB - AB_{con} \tag{35}$$

**Model B: calculations using Predici®**. Predici®, a commercial software developed and commercialized by CiT, has been used to study several RAFT polymerizations following the so-called Q-type approach.[19,37,38] In this approach, the main equilibrium between propagating radicals and dormant polymer are represented by introduction of species $Q(s)$ and $S(r)$, which keep track of the size of the two-arm adduct. The steps used in Predici® are listed in Table 5.[31,39] Regarding the mass transfer of low molar species (*LMS* = monomer, initiator or RAFT agent) and active radicals between the continuous and dispersed phases, Predici´s phase exchange and $k(s)$-termination steps, respectively, were implemented. Two phases were assumed from the beginning of the polymerization

in which the initial concentration for component "*LMS*" in phase $\Psi$ was calculated *via* partition coefficients defined as $\zeta_{LMS} = [LMS]_{dis}/[LMS]_{con}$ and used in the phase exchange step.[19] When using the $k(s)$-termination step, active radicals were assumed to remain in the continuous phase until they reach a critical length, given by a critical number-average chain-length ($\bar{P}_{nc}$). Eqn (19) was used thereafter. For simplification purposes, $k_{transferB}$ was assumed constant.[19] Recently, this model was used to study the RAFT polymerization of styrene in scCO₂. It was found that the predicted monomer concentration in both, continuous and dispersed phases, resemble those observed in typical solution polymerizations; accordingly, no diffusion-controlled effects are obversed.[20]
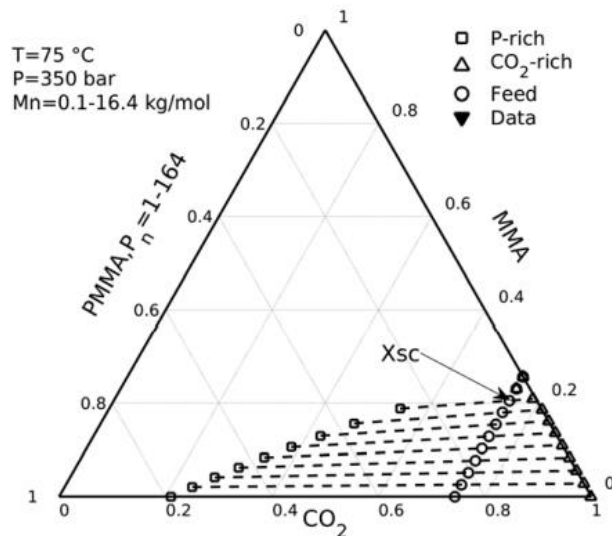


**Fig. 1**. Reaction path for case 1(see Table 6) using PC-SAFT parameters from Table 7.
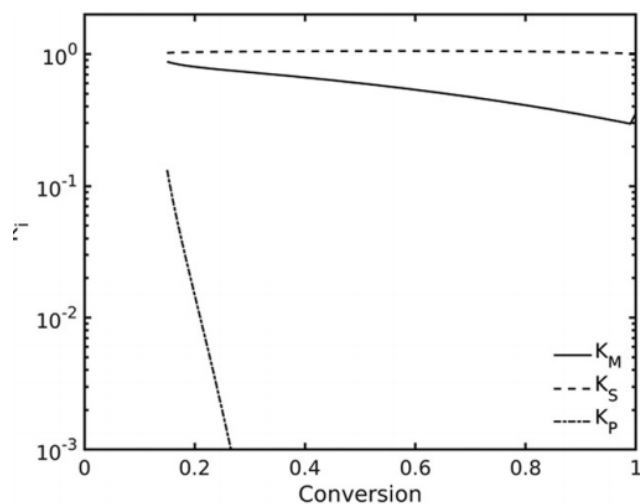
**Fig. 2** Equilibrium constant for monomers, solvent and oligomer as a function of monomer conversion for case 1 (see Table 6) using PC-SAFT parameters from Table 7.

## Model C: application of the PC-SAFT equation of state.

The PC-SAFT equation of state was derived assuming that molecules are conceived to be chains composed of spherical segments. Three pure-component parameters are used in PC-SAFT: segment diameter ($\sigma$), energy interaction parameter ($\varepsilon$) and number of segments ($m$).[28] The PC-SAFT equation of state has been used to correlate the sorption of supercritical fluids in polymers, to calculate cloud points for polymer/solvent mixtures and to calculate the phase behavior of copolymer systems.[27,40] In RAFT polymerization, most macromolecules are oligomers at low conversions. These species are expected to grow linearly with conversion. These species are expected to grow linearly with conversion, according to eqn (36).

$$\bar{P}_n = \frac{[M]_0 x}{[AB]_0} \tag{36}$$

Herein, PC-SAFT pure-component parameters for oligomers were interpolated assuming that parameter combinations $m$, $m\varepsilon/k$ and $m\sigma^3$ are linear with $\bar{P}_n$.[41] Thus, as observed in Fig. 1, the path of the reaction can be depicted in a ternary diagram taking into account eqn (36) and the mass balances for monomer, polymer and solvent, given by eqn (37)-(39), where $w_m$, $w_p$ and $w_s$ are masses of monomer, polymer and solvent, respectively.

$$w_m = w_{m0}(1 - x) \tag{37}$$

$$w_p = w_{m0}x \tag{38}$$

$$w_s = w_{s0} \tag{39}$$

**Table 6**     Initial conditions for RAFT polymerization of MMA using AIBN and TBTGA in scCO$_2$ (ref. 33)

| Case | $M/I/AB$ | $M/S$ | $t$ (°C) | $p$ (bar) |
|------|----------|-------|----------|-----------|
| 1 | 160/1/1 | 1/12 | 75 | 350 |
| 2 | 160/1/1 | 1/12 | 65-85 | 300 |
| 3 | 160/1/1 | 1/12 | 75 | 100-500 |

**Table 7**     Kinetic rate coefficients and free-volume parameters used in the simulations for non-RAFT reactions

| Kinetic rate coefficient or parameter | Unit | Value | Ref. |
|---------------------------------------|------|-------|------|
| $f_{con}$ | Dimensionless | 0.83 | [15] |
| $f_{dis}$ | Dimensionless | 0.5 | [15] |
| $k_{d,con}^0$ | s$^{-1}$ | $4.19 \times 10^{15} \exp(-16190/T)$ | [15] |
| $k_{d,dis}^0$ | s$^{-1}$ | $2.89 \times 10^{15} \exp(-15722/T)$ | [45] |
| $k_{p,con}^0 = k_{i,con}^0$ | L mol$^{-1}$ s$^{-1}$ | $5.2 \times 10^6 \exp((-3055 + 0.204(p - 1))T)$ | [15] |
| $k_{p,dis}^0 = k_{i,dis}^0$ | L mol$^{-1}$ s$^{-1}$ | $4.92 \times 10^5 \exp((-2190 + 0.204(p - 1))T)$ | [15] |
| $k_{t,\Psi}^0$ | L mol$^{-1}$ s$^{-1}$ | $9.8 \times 10^7 \exp((-349 - 0.1827(p - 1))T)$ | [15] |
| $k_{td,\Psi}^0/k_{tc,\Psi}^0$ | Dimensionless | $2.483 \times 10^3 \exp(-2057/T)$ | [46] |

| | | | |
|---|---|---|---|
| $T_{gM}, T_{gP}, T_{gS}$ | °C | -106, 114, -160 | [47] |
| $\alpha_M, \alpha_P, \alpha_s$ | °C$^{-1}$ | $1 \times 10^{-3}, 4.81 \times 10^{-4}, 7 \times 10^{-3}$ | [47] |
| $\beta_P, \beta_t, \beta_d$ | Dimensionless | $0.33, 1.45, 1 \times 10^{-3}$ | [47] |
| $\dfrac{m_M}{W_M}, \dfrac{m_P}{W_P}, \dfrac{m_S}{W_S}$ | mol g$^{-1}$ | 0.0306, 0.0262, 0.05839 | [30], [30],[44] |
| $\sigma_M, \sigma_P, \sigma_S$ | $10^{-10}$ m | 3.6238, 3.6, 2.5637 | [30], [30],[44] |
| $\dfrac{\varepsilon_M}{k_b}, \dfrac{\varepsilon_P}{k_b}, \dfrac{\varepsilon_S}{k_b}$ | K | 265.69, 245, 152.1 | [30], [30],[44] |
| $k_{MMA/CO_2}$ | Dimensionless | 0.05769 (50 °C), 0.07143 (60 °C), 0.06536 (70 °C), 0.06905 (80 °C), 0.06752 (50–80 °C) | This work |
| $k_{PMMA/CO_2}$ | Dimensionless | 0.10099 (50 °C), 0.10432 (65 °C), 0.10659 (80 °C | This work |
| $k_{MMA/PMMA}$ | Dimensionless | s −0.01 (65–80 °C) | This work |

It is observed in Fig. 1 that at low conversions ($0 \leq x < x_{sc}$) when oligomers are small and are present in minor amounts, the mixture is homogeneus until a limiting conversion $x_{sc}$ is reached; afterwards, a two-phases region is shown for $x > x_{sc}$.

**Table 8** Kinetic rate coefficients and free-volume parameters for RAFT reactions used in the simulations corresponding to case 1 (T=75 °C and P=350 bar)

| Kinetic constant or parameter | Units | Value (model A) | Value (model B) | Value (model C) |
|---|---|---|---|---|
| $k^0_{add,\Psi} = k^0_{\_bd,\Psi}$ | L mol$^{-1}$ s$^{-1}$ | $2.6 \times 10^5$ | $2.6 \times 10^5$ | $2.6 \times 10^5$ |
| $k^0_{\_add,\Psi} = k^0_{bd,\Psi}$ | s$^{-1}$ | $2.6 \times 10^1$ | $2.6 \times 10^1$ | $2.6 \times 10^1$ |
| $k^0_{a,\Psi} = k^0_{\_b,\Psi}$ | L mol$^{-1}$ s$^{-1}$ | $2.6 \times 10^5$ | $2.6 \times 10^5$ | $2.6 \times 10^5$ |
| $k^0_{\_a,\Psi} = k^0_{b,\Psi}$ | s$^{-1}$ | $2.6 \times 10^1$ | $2.6 \times 10^1$ | $2.6 \times 10^1$ |
| $k^0_{tir,\Psi}$ | L mol$^{-1}$ s$^{-1}$ | $2.6 \times 10^6$ | $1.2 \times 10^6$ | $2.6 \times 10^6$ |
| $x_c, K_s$ | s$^{-1}$ | 0.95, 0.3 | Not used | Not used |
| $\zeta_M, \zeta_I, \zeta_{AB,} \zeta_{CO_2}$ | Dimensionless | Not used | 2, 2, 2, 0.5 | Not used |
| $\zeta_{P,}$ | Dimensionless | $2 \times 10^2$ | Not used | $2 \times 10^2$ |
| $k_{pe}$ | min$^{-1}$ | Not used | $1 \times 10^{-2}$ | Not used |
| $k_{transferA,\Psi}$ | min$^{-1}$ | $1 \times 10^{-4}$ | Not used | $1 \times 10^{-4}$ |
| $k_{transferB,\Psi}$ | min$^{-1}$ | Not used | $1 \times 10^2$ | Not used |

| $\beta_{add}, \beta_{\_add}, \beta_a, \beta_{\_a}$ | Dimensionless | 0.5, 0.2, 0.5, 0.2, 0.2 |
|---|---|---|

The equilibrium constants defined as $K_i = X_{i,con}/X_{i,dis}$ depend on monomer conversion, as shown in Fig. 2. As mentioned above, in the description of model A, the partition of monomer and initiator were calculated with eqn (32)-(35).

**Diffusion-controlled effects**

Diffusion-controlled effects (DCEs) for all the reactions involving polymer molecules were modeled using free-volume theory, according to eqn (40), where $k_i$ is effective kinetic rate coefficient, and $k_i^0$ is the corresponding intrinsic kinetic rate coefficient. $V_{f0}$ is fractional free volume at initial conditions; $V_f$ is fractional free volume at time $t$; and $\beta_i$ is a free volume parameter. Fractional free volume was calculated using eqn (41), where $\alpha_n$, $T_{gn}$ and $\varphi_n$ are expansion coefficient, glass transition temperature and volume fraction for component $n$, respectively.[20,42]

$$k_i = k_i^0 \exp\left[-\beta_i\left(\frac{1}{V_f} - \frac{1}{V_{f0}}\right)\right] \tag{40}$$

$$Vf = 0.025 + \sum_{n=1}^{\#of\,components} \alpha_n(T - T_{gn})\phi_n \tag{41}$$

It should be noted that eqn (40) and (41) are applied only to the dispersed phase since DCEs are usually negligible at low concentrations. In a previous work, a set of reasonable partition coefficients used in model B resulted in small variations of free-volume in the dispersed phase. In contrast, significant DCEs were observed when model A was used.[20] The variation of free-volume was monitored in all models.

**Table 9**      Upper boundary (limiting conversion) of stage 1 ($x_{sa} = x_{sc}$) employed in models A and C

| $T$ (°C) | $p$ (bar) | $x_{sa}$ | $T$ (°C) | $p$ (bar) | $x_{sa}$ |
|---|---|---|---|---|---|
| 75 | 100 | 0.00 (L-V) | 75 | 450 | 0.20 |
| 75 | 150 | 0.06 | 75 | 500 | 0.23 |
| 75 | 200 | 0.08 | 65 | 300 | 0.15 |
| 75 | 250 | 0.10 | 70 | 300 | 0.13 |
| 75 | 300 | 0.12 | 75 | 300 | 0.12 |
| 75 | 350 | 0.15 | 80 | 300 | 0.11 |
| 75 | 400 | 0.17 | 85 | 300 | 0.11 |

**Numerical implementation**

Models A and C result in sets of ordinary differential equations (ODEs) which were implemented and solved using the C programming language in a supercomputer with Intel® compilers (Miztli, UNAM, Mexico). Sundials' CVODE routine was employed, using backward differentiation with both absolute and relative tolerances set to 10^{-12}.[43] The PC-SAFT binary interaction parameters were estimated using Aspen Plus® version 8.8;[44] whereas the L-L equilibrium was calculated using software VLXE (www.vlxe.com). Model B was implemented in Predici®, version 7, using a desktop computer with an Intel Core 2® Quad processor and 4 GB of RAM. Numerical integration of ODEs using models A and C took less than 1 minute, whereas the simulation times for model B required from 1 to 4 hours. Computational times of interaction parameters and L-L equilibrium using ASPEN Plus and VLXE, respectively, took less than 1 minute for each case study.

RESULTS AND DISCUSSION

As summarized in Table 6, three cases corresponding to RAFT polymerization of MMA using AIBN and *S*-thiobenzoyl thioglycolic acid (TBTGA) in scCO$_2$, are analyzed in this contribution.[33] The kinetic rate coefficients and physicochemical parameters used in the simulations are listed in Tables 7 and 8.

**Table 10**     Kinetic rate coefficients for RAFT reactions used in the simulations corresponding to case 1 in Fig. 6 (T=75 °C and P=350 bar)

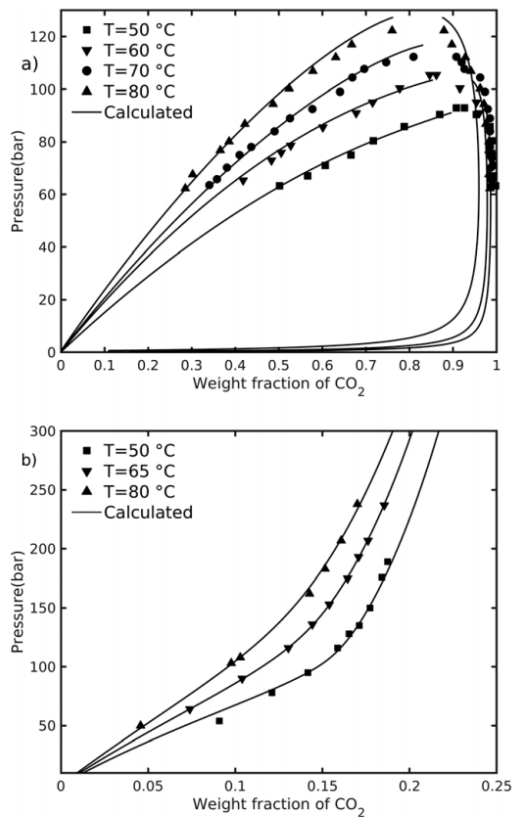| Kinetic constant or | Units | Value (model C) | Value (model C2) |
|---|---|---|---|
| $k^0_{add,\Psi} = k^0_{\_bd,\Psi}$ | L mol$^{-1}$ s$^{-1}$ | $2.6 \times 10^5$ | $1.4 \times 10^5$ |
| $k^0_{\_add,\Psi} = k^0_{bd,\Psi}$ | s$^{-1}$ | $2.6 \times 10^1$ | $1.4 \times 10^1$ |
| $k^0_{a,\Psi} = k^0_{\_b,\Psi}$ | L mol$^{-1}$ s$^{-1}$ | $2.6 \times 10^5$ | $1.4 \times 10^5$ |
| $k^0_{\_a,\Psi} = k^0_{b,\Psi}$ | s$^{-1}$ | $2.6 \times 10^1$ | $1.4 \times 10^1$ |
| $k^0_{tir,\Psi}$ | L mol$^{-1}$ s$^{-1}$ | $2.6 \times 10^6$ | $1.4 \times 10^6$ |
| $\zeta_P$ | Dimensionless | $2 \times 10^2$ | $2 \times 10^2$ |
| $k_{transferA,\Psi}$ | min$^{-1}$ | $1 \times 10^{-4}$ | $1 \times 10^{-5}$ |

**Fig. 3** Comparison of experimental data and calculated profiles of pressure *versus* weight fraction of $CO_2$: a) L-L equilibria of MMA/$CO_2$ and b) sorption of $CO_2$ into PMMA.

As explained in Model C: application of the PC-SAFT equation of state, limiting conversions for stage 1 in models A and C ($x_{sa}$, $x_{sc}$, respectively) were estimated following the development of $\bar{P}_n$ with monomer conversion (see Fig. 1). Limiting conversions at different temperatures and pressures are summarized in Table 9. On the other hand, in model B the *LMS* partition coefficients used in the "phase exchange" step of Predici were set to reasonable values, namely, $\zeta_M = \zeta_I = \zeta_{AB} = 2$ and $\zeta_S = 0.4$.
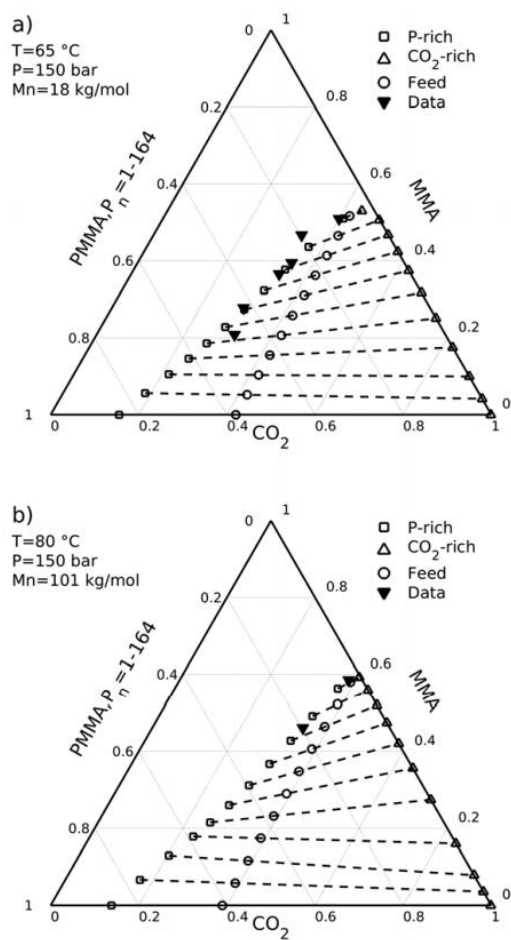
**Fig. 4** Comparison of L-L equilibrium experimental data and calculated values for ternary system PMMA/MMA/$CO_2$ at: a) T=65 °C and 150 bar, with $\overline{M_w}$=18 kg mol$^{-1}$, and b) T=80 °C and 150 bar, with $\overline{M_w}$=101 kg mol$^{-1}$
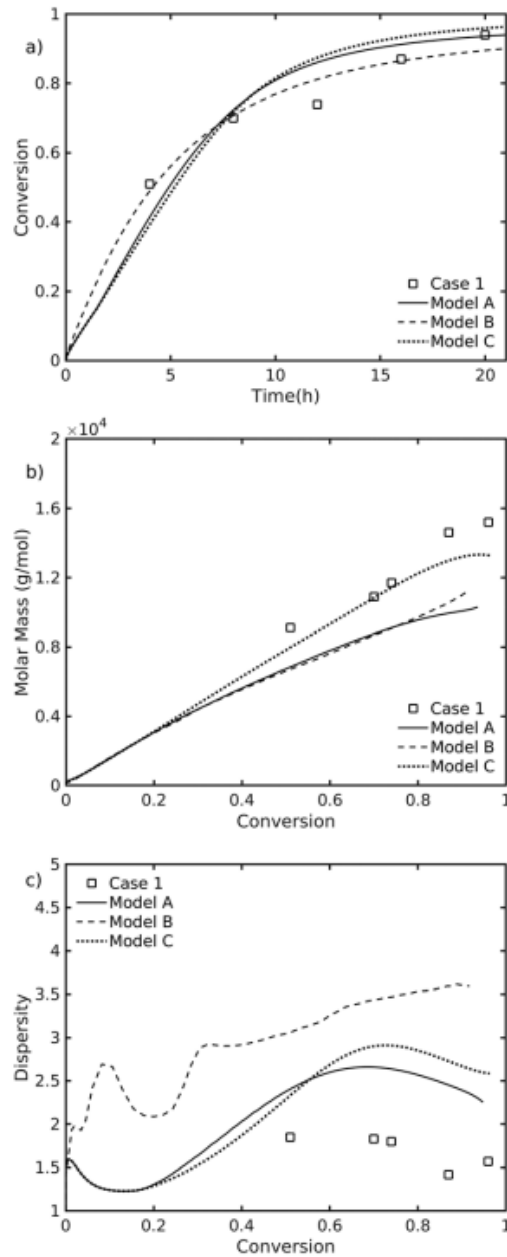
**Fig. 5**. Comparison of experimental data and predicted profiles of polymerization rate and molar mass development using model A, B and C: a) monomer conversion *versus* time, b) Mn *versus* conversion and c) Ð *versus* conversion.

These values were chosen assuming that the concentrations of reactants are higher in the dispersed phase. Critical chain-lengths used in the "$k(s)$-termination" step were estimated as $\bar{P}_{nc} = x_{sa}[M]_0/[AB]_0$. The obtained values of $x_{sa}$ are summarized in Table 9.

The PC-SAFT binary interaction parameters, $k_{ij}$, employed in model C for MMA/$CO_2$, PMMA/$CO_2$ and MMA/$CO_2$ were fitted to L-V experimental data[48] and L-L[30,49] equilibria, as observed in Fig. 3 and 4. It should be noted that the estimated PC-SAFT parameters for $CO_2$ are different from those used by Görnert and Sadowski, who used different L-V experimental data for the estimation of $k_{ij}$ values for MMA/$CO_2$ were obtained in this work, but the estimated parameters for PMMA/$CO_2$ and MMA/PMMA are similar.

Case 1 was used to compare the performance of models A, B and C at 75°C and 350 bar. The predicted profiles of monomer conversion *versus* time (a), $\bar{M}_n$ *versus* conversion (b), and Đ *versus* conversion (c) are compared against the corresponding experimental data in Fig. 5. As reported in Table 8, the values of $k_{a,\psi}^0$, $k_{-a,\psi}^0$ and $k_{tir,\psi}^0$ used in the simulations were practically the same. Those values provided the best results for each model. The fitted value of $k_{tir,\psi}^0$ for model B resulted in a slightly lower value, compared to that for models A and C.
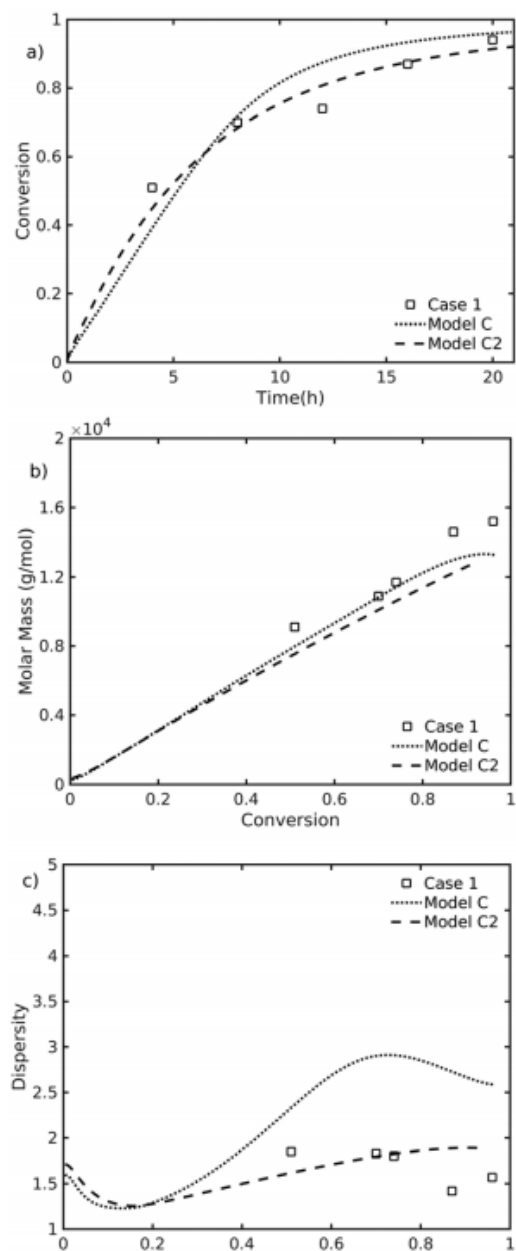
**Fig. 6** Comparison of experimental data and predicted profiles of polymerization rate and molar mass development using model C and C2: a) monomer conversion *versus* time, b) $\overline{M_n}$ *versus* conversion and c) *Đ versus* conversion.
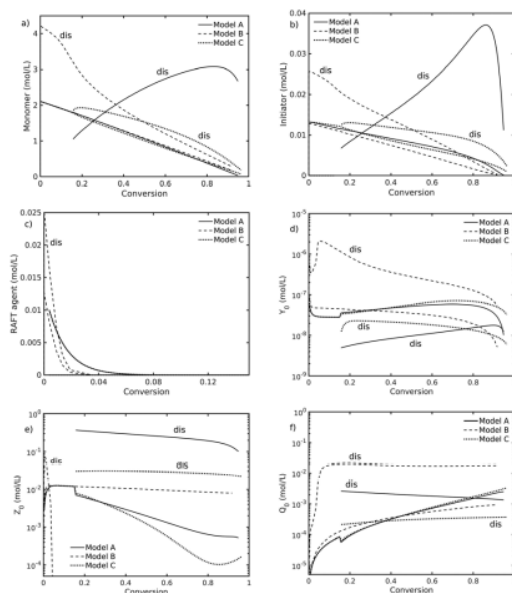
Fig. 7 Comparison of predicted profiles of concentrations *versus* conversion for: a) monomer, b) initiator, c) RAFT agent, d) living polymer, e) dormant polymer, and f) dead polymer, using models A, B and C.

The calculated profiles of conversion *versus* time agree well with experimental data, especially the one calculated with model B, as observed in Fig. 5a. It is observed in Fig. 5b that model C captures nicely the linear behavior of $\bar{M}_n$ *versus* conversion up to about 80% monomer conversion, where slight underprediction starts to appear. The underprediction region of the $\bar{M}_n$ *versus* conversion profile appears earlier in models A and B. All the calculated profiles of Đ *versus* conversion lie above the experimental data, as observed in Fig. 5c. It is expected in RDRP systems that Đ values are low, and not greater than 2. The profiles shown in Fig. 5 are the best results when conversion and $\bar{M}_n$ data are used for parameter estimation purposes. However, a better description of Đ can be provided by model C if different kinetic parameters (identified as model C2 in Table 10) are used, as observed in profile C2 in Fig. 6. Masoumi *et al.* used the sequential Bayesian Monte Carlo model discrimination method to RAFT polymerization and concluded than $\bar{M}_n$ is a suitable

process output for model discrimination purposes but it was not enough to discriminate models of similar mathematical structures as the ones compared in this study.[50] They pointed out that more experimental information, such as the concentration of intermediate radicals, $R(s)AR_\Psi(r)$, was necessary fur such as purposes.[50] Therefore, more experimental data such as intermediate species and three-arm dead polymer concentrations would be necessary to adequately discriminate between models A, B and C.

Predicted profiles of concentrations of monomer, initiator, RAFT agent, active radicals $(Y_0)$, dormant polymer $(Z_0)$ and dead polymer by combination and termination $(Q_0)$ for case 1, using models A, B and C, are shown in Fig. 7. It is observed in Fig. 7a that the predicted monomer concentration profiles in the continuous phase are very similar, while those in the dispersed phase behave differently. Similar trends were obtained for the initiator, as observed in Fig. 7b. As expected, the RAFT agent is completely consumed during the first stages of reaction, mostly in the continuous phase, in the low conversion range $x \leq 0.1$.

**Influence of temperature on RAFT polymerization of MMA in scCO$_2$**

The effect of temperature on polymerization rate and molar mass development in RAFT polymerizations has been addressed by some groups in the open literature. Hernández-Ortiz *et al.*[51] estimated $k_a$, $k_b$ and $k_{tir}$ for the RAFT polymerization of styrene using 2-cyanoprop-2-yl 1-dithionaphtalate (CPDN) and AIBN at 60, 72 and 98°C. The kinetic rate coefficients were found to vary one order of magnitude when operating between 60 to 98 °C. For instance, $k_a = 2 \times 10^5$, $8 \times 10^5$ and $2 \times 10^6$ at 60, 72 and 98 °C, respectively. Meiser *et al.*[52] estimated $K_{eq} = k_a/k_b$ for the RAFT polymerization of butyl acrylate (BA) using *S*-thiobenzoyl-2-thiopropionate (ETTP) *via* single fast electron paramagnetic resonance (EPR), scanning in a range between -40 and 70 °C. They obtained an activation energy of $E(K_{eq})$ = -49.5 kJ mol$^{-1}$, and assuming that $E(k_a)$ = 8.4 kJ mol$^{-1}$, it was estimated that $E(k_b)$ = 57.9 kJ mol$^{-1}$, that is, $k_b$'s activation energy is about 7 times greater than that of $k_a$.[52]
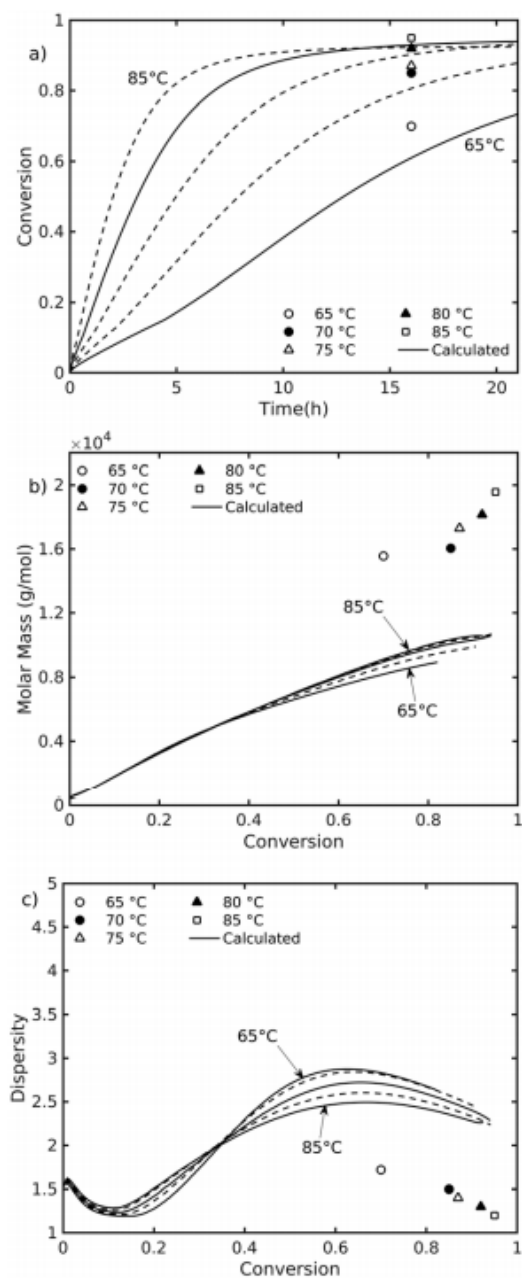
**Fig. 8** Comparison of experimental data and calculated profiles of: a) monomer conversion *versus* time, b) $\overline{M_n}$ *versus* conversion, and c) Đ *versu*s conversion, using model A at 300 bar and 65, 70, 75, 80 and 85 °C.
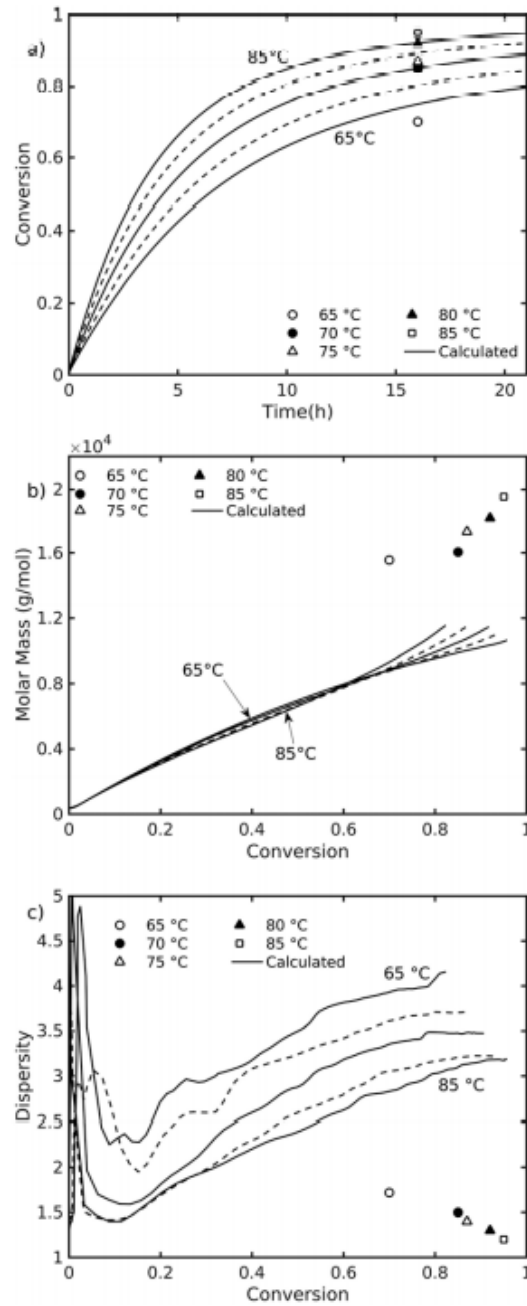
Fig. 9 Comparison of experimental data and calculated profiles of: a) monomer conversion *versus* time, b) Mn *versus* conversion, and c) Đ *versus* conversion, using model B at 300 bar and 65, 70, 75, 80 and 85 °C.

Herein, the activation energy of $k_a$ was set to a low value of $E(k_a)$ = 8.4 kJ mol$^{-1}$,[53] the activation energy of $k_b$ was assumed to be four times greater than that of $k_a$, $E(k_b)$ = $4E(k_a)$, and the activation energy of $k_{tir}$ was considered to be the same as that of $k_t$, namely, $E(k_{tir})$ = $E(k_t)$. Comparison of experimental data and

calculated profiles of monomer conversion *versus* time, $\bar{M}_n$ *versus* conversion and

Đ *versus* conversion at 300 bar and 65, 70, 75, 80 and 85 °C, using models A, B and

C are shown in Fig. 8-10, respectively. It should be noted that parameters $x_c$, $K_{sc}$

and $\zeta_M$, $\zeta_I$, $\zeta_{AB}$, $\zeta_{CO_2}$, used in models A and B, respectively, were kept constant in the

temperature and pressure ranges studied in the present and following subsections.
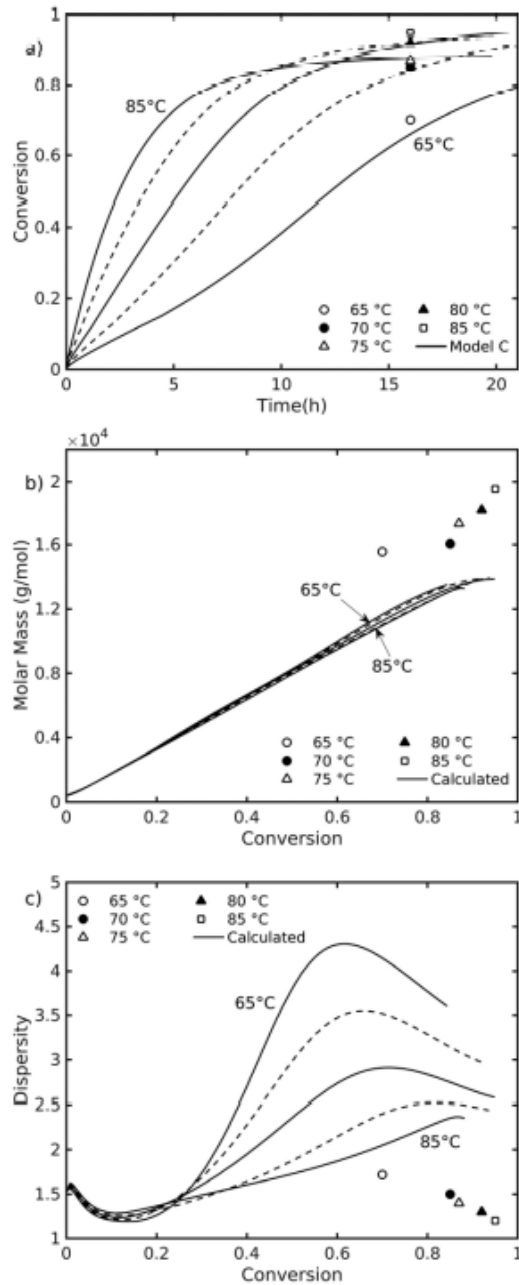
**Fig. 10** Comparison of experimental data and calculated profiles of: a) monomer conversion *versus* time, b) $\overline{M_n}$ *versus* conversion, and c) Đ *versus* conversion, using model C at 300 bar and 65, 70, 75, 80 and 85 °C.

As expected, high temperatures lead to high polymerization rates, mainly at the beginning of the polymerizations. It is observed in Fig. 8 and 10 that no significant increase in final monomer conversion at temperatures higher than 75 °C is predicted by models A and C, and a gradual increase is obtained by model B (see Fig. 9). The

calculated profiles of $\bar{M}_n$ *versus* conversion vary only slightly when going from 65 to 85 °C. Finally, the calculated Đ values decrease as temperature increases, following the experimental trends.

**Influence of pressure on RAFT polymerization of MMA in scCO₂**

Regarding the pressure dependence of parameters $k_a$, $k_b$ and $k_{tir}$, it was assumed that their activation volumes $(V^{\neq})$ are related to those of the propagation and termination reactions as follows: $V^{\neq}(k_a) = V^{\neq}(k_b) = V^{\neq}(k_p)$= -16.7 cm$^3$ mol$^{-1}$, and $V^{\neq}(k_{tir}) = V^{\neq}(k_t)$ = 15.0 cm$^3$ mol$^{-1}$.[15] Comparison of experimental data and calculated profiles of monomer conversion *versus* time, $\bar{M}_n$ *versus* conversion and *Đ versus* conversion using models A, B and C at 75 °C and 100 to 500 bar are shown in Fig. 11-13, respectively. As shown in Table 9, higher pressures favor solubility of oligomers. It is observed in Fig. 11-13a that higher monomer conversions are attained at higher pressures and the final conversion range is broader when model C is used. $\bar{M}_n$ is predicted to increase with pressure by models A and B. Model C predicts a slight decrease, instead, which agrees better with experimental data, as observed in Fig. 11-13b. Đ values are predicted to decrease with pressure when models A and C are used; on the other hand, model B predicted an increasing behavior of Đ. It is interesting to note that at the beginning of the polymerization, the MMA/CO₂ mixture at 75 °C and 100 bar consists of two phases, liquid and vapor. It is therefore expected that the predictions for this case may be inaccurate. This is indeed confirmed in Fig. 13, where it is observed that the predicted profiles at 100 and 150 bar deviate significantly from the other cases.
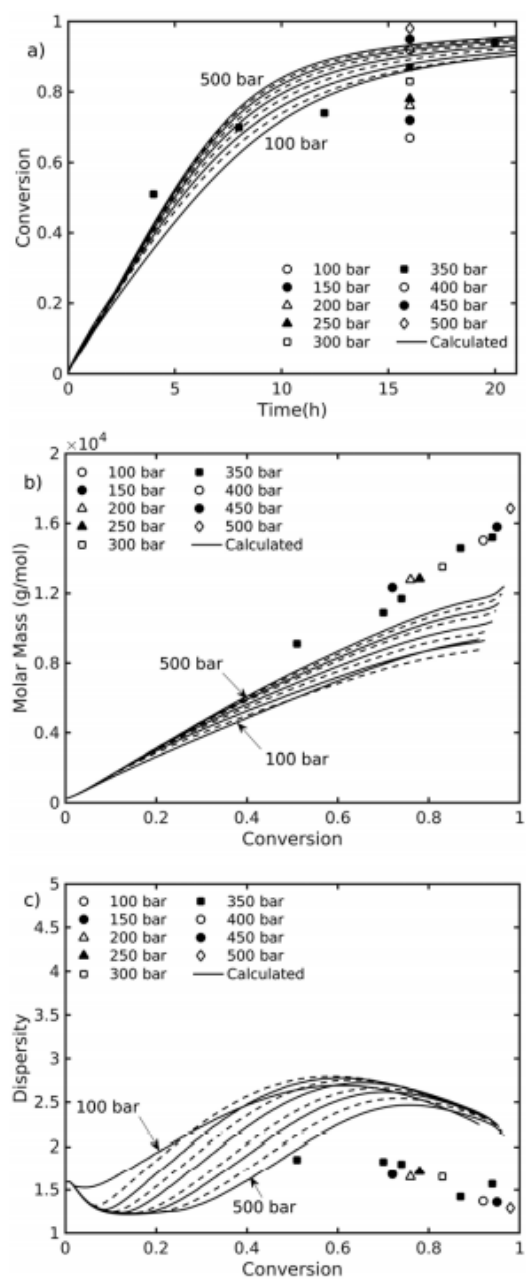
**Fig. 11**    Comparison of experimental data and calculated profiles of: a) monomer conversion *versus* time, b) Mn *versus* conversion, and c) Đ *versus* conversion, using model A at 75 °C and 100 to 500 bar.
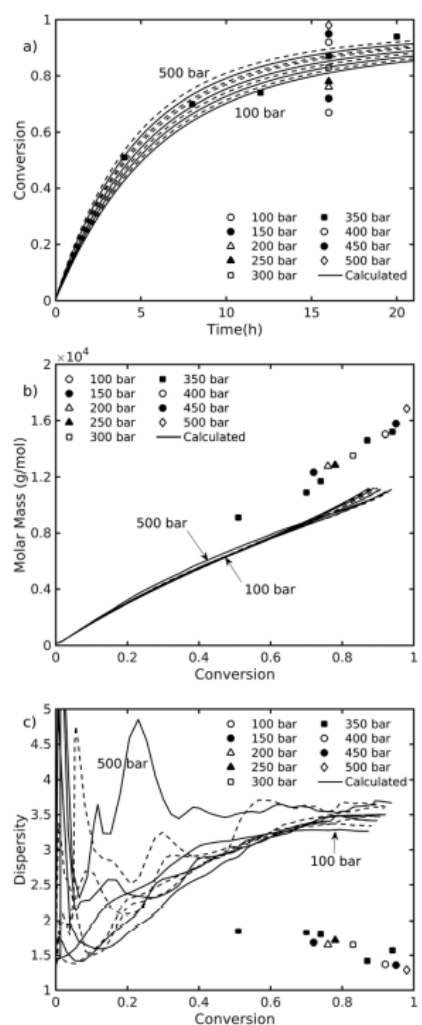
Fig. 12    Comparison of experimental data and calculated profiles of: a) monomer conversion *versus* time, b) $\overline{M_n}$ *versus* conversion, and c) Ð *versus* conversion, using model B at 75 °C and 100 to 500 bar.

CONCLUSIONS

Three modeling approaches were used to analyze the kinetics of RAFT polymerization of MMA in scCO$_2$, using AIBN and TBTGA in a range of temperatures and pressures of 65-85 °C and 100-500 bar, respectively. The method of moments was used in models A and C to simplify the polymer material balances. In model B the reaction mechanism was implemented in the Predici® software.

46

Regarding the partition of monomer and solvent between continuous and dispersed phases, semi-empirical equations were used in model A; in model B, Predici´s "phase exchange" and "$k(s)$-termination" steps were used; and in model C, such calculations were carried out using the PC-SAFT equation of state.
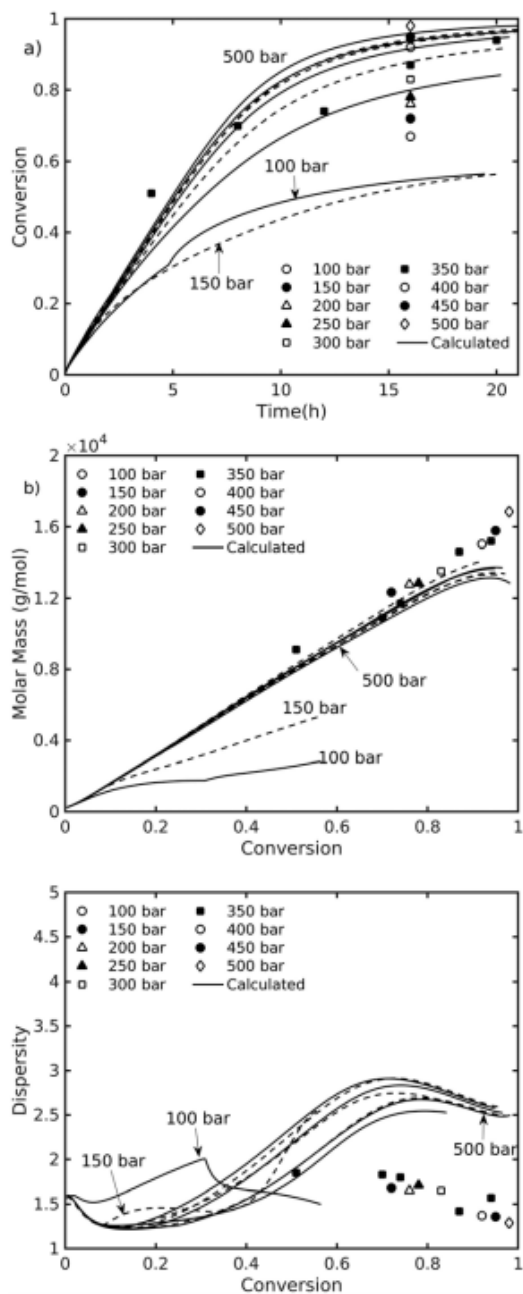
**Fig. 13**   Comparison of experimental data and calculated profiles of: a) monomer conversion *versus* time, b) $\overline{M_n}$ *versus* conversion, and c) Đ *versus* conversion, using model C at 75 °C and 100 to 500 bar.

As a fundamental tool, the PC-SAFT equation of state allowed to estimate the monomer conversion $(x_s)$ at which oligomers of size $\bar{P}_n$ become insoluble in $CO_2$. In most cases, the polymerizations were carried out in two stages. First, the system was assumed to be homogeneous and proceeded as a solution polymerization until

a conversion $x_s$ is reached, when a second phase is formed and the polymerization proceeds as a heterogeneous system.

All models captured well the temperature effect on the polymerization performance, in the range 65-85 °C. Regarding the pressure effect, it was found that simulations at low pressures may not satisfactorily represent the polymerization kinetics, especially at 100 bar, since the polymerization at such conditions starts as a liquid-vapor mixture.

The profiles of monomer concentration in the dispersed phase did not show significant diffusion-controlled effects. Overall, the application of PC-SAFT equation of state allowed a better understanding of the process.

NOMENCLATURE

| | |
|---|---|
| [ ] | Denotes molar concentration, mol L$^{-1}$ |
| $AB_\Psi$ | Moles or concentration of RAFT agent in phase $\Psi$, mole per L |
| $B_\Psi^\cdot$ | Moles or concentration of primary radical from fragmentation of the RAFT agent ("R" leaving group of the RAFT molecule), mol L$^{-1}$ |
| Đ | Molar mass dispersity, dimensionless |
| $E_{m,\Psi}$ | m-th moment of the one-arm adduct polymer population in phase $\Psi$ ($m$ = 0, 1, 2, …), mol L$^{-1}$ |
| $f_\Psi$ | Chemical initiator efficiency in phase $\Psi$ |
| $F_{mn,\Psi}$ | Moment of order $m$ on one arm and $n$ on the other of the two-arm adduct polymer population, in phase $\Psi$ ($m$, $n$ = 0, 2, 2, …), mol L$^{-1}$ |
| $G_{mnu,\Psi}$ | Moment of order m on one arm, $n$ on the second arm and $u$ on the third one of the three-arm dead polymer population, in phase $\Psi$ ($m$, $n$, $u$ = 0, 1, 2, …), mol L$^{-1}$ |
| $I_\Psi$ | Moles or concentration of initiator in phase $\Psi$, mol L$^{-1}$ |
| $k_{ij}$ | Binary interaction parameter |
| $k_{a,\Psi}^0$ | Intrinsic kinetic rate coefficient for the forward fragmentation step of the chain equilibration reaction in phase $\Psi$, L mol$^{-1}$ s$^{-1}$ |
| $k_{-a,\Psi}^0$ | Intrinsic kinetic rate coefficient for the reverse fragmentation step of the chain equilibration reaction in phase $\Psi$, L mol$^{-1}$ s$^{-1}$ |
| $k_{add,\Psi}^0$ | Intrinsic kinetic rate coefficient for the forward addition step of the reversible chain transfer to RAFT agent reaction in phase, L mol$^{-1}$ s$^{-1}$ |
| $k_{-add,\Psi}^0$ | Intrinsic kinetic rate coefficient for the reverse fragmentation step of the reversible chain transfer to RAFT agent in phase $\Psi$, s$^{-1}$ |
| $k_{b,\Psi}^0$ | Intrinsic kinetic rate coefficient for the forward fragmentation step of the chain equilibration reaction in phase $\Psi$, s$^{-1}$ |
| $k_{-b,\Psi}^0$ | Intrinsic kinetic rate coefficient for the reverse addition step of the chain equilibration reaction in phase, L mol$^{-1}$ s$^{-1}$ |

| | |
|---|---|
| $k_{bd,\Psi}^0$ | Intrinsic kinetic rate coefficient for the forward fragmentation step of the reversible chain transfer to RAFT agent in phase $\Psi$, s$^{-1}$ |
| $k_{-bd,\Psi}^0$ | Intrinsic kinetic rate coefficient for the reverse addition step of the reversible chain transfer to RAFT agent in phase, L mol$^{-1}$ s$^{-1}$ |
| $k_{d,\Psi}^0$ | Intrinsic kinetic rate coefficient for decomposition in phase $\Psi$, s$^{-1}$ |
| $k_{i,\Psi}^0$ | Intrinsic kinetic rate coefficient for first propagation in phase $\Psi$, L mol$^{-1}$ s$^{-1}$ |
| $k_{p,\Psi}^0$ | Intrinsic kinetic rate coefficient for propagation in phase $\Psi$, L mol$^{-1}$ s$^{-1}$ |
| $k_{pe}$ | LMS phase transfer coefficient, min$^{-1}$ |
| $k_b$ | Boltzman constant, $1.38064 \; x \; 10^{-23}$ J K$^{-1}$ |
| $k_{t,\Psi}^0$ | Intrinsic kinetic rate coefficient for termination in phase $\Psi$, L mol$^{-1}$ s$^{-1}$ |
| $k_{tc,\Psi}^0$ | Termination by combination intrinsic kinetic rate coefficient in phase $\Psi$, L mol$^{-1}$ s$^{-1}$ |
| $k_{td,\Psi}^0$ | Termination by disproportion intrinsic kinetic rate coefficient in phase $\Psi$, L mol$^{-1}$ s$^{-1}$ |
| $k_{tir,\Psi}^0$ | Intermediate radical termination by disproportion intrinsic kinetic rate coefficient in phase $\Psi$, L mol$^{-1}$ s$^{-1}$ |
| $k_{transferA,\Psi}$ | Mass transfer coefficient in phase $\Psi$ , used in models A and C, min$^{-1}$ |
| $k_{transferB,\Psi}$ | Mass transfer coefficient in phase $\Psi$, used in models B, min$^{-1}$ |
| $k_{j,\Psi}$ | Effective kinetic rate coefficient for reaction $j$ in phase $\Psi$ |
| $K_i$ | Equilibrium constant for the $i$-th reaction |
| $K_s$ | Solubility constant of solvent ($CO_2$) in monomer mixture |
| *LMS* | Low molar species (M, AB and I) |
| $m$ | Number of segments PC-SAFT parameters |
| $M_\Psi$ | Moles or concentration of monomer in phase $\Psi$, mol L$^{-1}$ |
| $p$ | Pressure, bar (unless indicated otherwise) |

$P_\Psi(s)$      Moles or concentration of dead polymer species of size $s$ in phase $\Psi$, mol L$^{-1}$

$Pol_\Psi(s)$      Moles or concentration of polymer species of size $s$ in phase $\Psi$, mol L$^{-1}$

$PA_\Psi(s)$      Moles or concentration of dormant polymers of size $s$ in phase $\Psi$, mol L$^{-1}$

$\bar{P}_n$      Number-average chain length

$\bar{P}_{nc}$      Critical number-average chain lenght

$\bar{P}_w$      Weight-average chain length

$Q(s)$      Moles or concentration of two-arm adduct of size $s$ used in model B, mol L$^{-1}$

$Q_{m,\Psi}$      $m$-th moment of the polymer population produced by termination by disproportion in phase $\Psi$ ($m$ = 0, 1, 2, …), mol L$^{-1}$

$R^*_{in,\Psi}$      Moles or concentration of primary free radicals in phase $\Psi$, mol L$^{-1}$

$R_\Psi(s)$      Moles or concentration of active radicals of size $s$ in phase $\Psi$, mol L$^{-1}$

$R_\Psi(s)AB$      Moles or concentration of one-arm adduct of size $s$ in phase $\Psi$, mol L$^{-1}$

$R(s)AR_\Psi(r)$      Moles or concentration of two-arm adduct of size $s$ and dormant polymer of size $r$, mol L$^{-1}$

$S(r)$      Moles or concentration of two-arm adduct of size $r$ used in model B, mole per L

$t$      Time, s (unless indicated otherwise)

$T$      Temperature, K (unless indicated otherwise)

$T(s)$      Moles or concentration of three-arm dead polymer of size $s$, mol L$^{-1}$

$T_{gi}$      Glass transition temperature for component I, K

$V_{f0}$      Fractional free volume at initial conditions, dimensionless

$V_{f0}$      Fractional free volume, dimensionless

$V^{\neq}$      Activation volume, cm$^3$ mol$^{-1}$

$V_\Psi$      Volume of phase $\Psi$, cm$^3$

| | |
|---|---|
| $w_i$ | Mass of component i (i = M, P and S), g |
| $W_i$ | Molar mass of component i (i = M, P and S), g mol$^{-1}$ |
| $x$ | Monomer conversion, dimensionless |
| $x_c$ | Critical conversion, dimensionless |
| $x_{sa}$ | Limit solubility conversion in model A, dimensionless |
| $x_{sc}$ | Limit solubility conversion in model C, dimensionless |
| $X_{i,\Psi}$ | Molar fraction of component i phase Ψ, dimensionless |
| $Y_{m,\Psi i}$ | $m$-th moment of the living polymer population in phase Ψ ($m$ = 0, 1, 2, …), dimensionless |
| $Z_{m,\Psi}$ | $m$-th moment of the dormant polymer population in phase Ψ ($m$ = 0, 1, 2, …), dimensionless |

GREEK LETERS

| | |
|---|---|
| $\alpha_i$ | Parameter for calculation of free volume expansion coefficient, °C$^{-1}$ |
| $\beta_j$ | Free volume parameter for reaction $j$ |
| $\varepsilon$ | Energy interaction parameter, J |
| $\zeta_i$ | Partition coefficient (i = LMS or polymer) |
| $\zeta_P(s)$ | Partition coefficient for polymer species of size $s$ |
| $\mu_{m,\Psi}$ | $m$-th moment of the total polymer population in phase Ψ ($m$ = 0, 1, 2, …), mol L$^{-1}$ |
| $\sigma$ | Segment diameter, m |
| $\varphi_i$ | Volume fraction for component i |
| Ψ | Reacting phase, Ψ = con (dis) for continuous (dispersed) phase |
| $\Psi_2$ | Second reacting phase |

CONFLICTS OF INTEREST

There are no conflicts to declare.

NOTES AND REFERENCES

1  P. B. Zetterlund, F. Aldabbagh and M. Okubo, J. *Polym. Sci.*, P*art A: Polym. Chem.*, 2009, **47**, 3711–3728.

2  M. F. Cunningham, *Prog. Polym.* Sci., 2008, **33**, 365–398.

3  G. Moad, E. Rizzardo and S. H. Thang, *Aust. J. Chem.*, 2012, **65**, 985–1076.

4  G. Moad, *J. Polym. Sci., Part A: Polym. Chem.*, 2019, **57**, 216–227.

5  P. R. Rodrigues and R. P. Vieira, *Eur. Polym. J.*, 2019, **115**, 45–58.

6  P. Chmielarz, M. Fantin, S. Park, A. A. Isse, A. Gennaro, A. J. D. Magenau, A. Sobkowiak and K. Matyjaszewski, *Prog. Polym. Sci.*, 2017, **69**, 47–78

7  E. Vivaldo-Lima, G. Jaramillo-Soto and A. Penlidis, in *Encyclopedia of Polymer Science and Technology*, Wiley, New York, 2016, pp. 1–48, DOI: 10.1002/0471440264.pst648.

8  A. Simula, N. Ballard, M. Aguirre, J. R. Leiza, S. v. Es and J. M. Asua, *Eur. Polym. J.*, 2019, **110**, 319–329.

9  X. Wang, L. Shen and Z. An, *Prog. Polym. Sci.*, 2018, **83**, 1–27.

10 G.-X. Wang, M. Lu, Z.-H. Hou, Y. Gao, L.-C. Liu and H. Wu, *J. Appl. Polym. Sci.*, 2014, **131**(7), 40135.

11 Z. Y. Huo, P. D. Xia, U. Azhar, J. C. Ma, X. M. Zhang, X. Y. Zhou, S. X. Zhang and A. H. Xu, *IOP Conf. Ser.: Mater. Sci.* Eng., 2019, **479**, 012107.

12 J. Jennings, M. Beija, J. T. Kennon, H. Willcock, R. K. O'Reilly, S. Rimmer and S. M. Howdle, *Macromolecules*, 2013, **46**, 6843–6851.

13 J. Wieme, D. R. D'hooge, M.-F. Reyniers and G. B. Marin, *Macromol. React. Eng.*, 2009, **3**(1), 16–35.

14 M. Zhang and R. A. Hutchinson, *Macromol. React. Eng.*, 2018, **12**(5), 1800025

15 P. A. Mueller, G. Storti and M. Morbidelli, *Chem. Eng. Sci.*, 2005, **60**, 1911–1925.

16 C. Chatzidoukas, P. Pladis and C. Kiparissides, *Ind. Eng. Chem. Res.*, 2003, **42**, 743–751.

17 L. I. Costa, G. Storti, M. Morbidelli, L. Ferro, O. Scialdone, G. Filardo and A. Galia, *Macromolecules*, 2010, **43**, 9714–9723.

18 C. Kiparissides, *Adv. Polym. Sci.*, 2018, **280**, 121–193.

19 G. Jaramillo-Soto, M. L. Castellanos-Cárdenas, P. R. GarcíaMorán, E. Vivaldo-Lima, G. Luna-Bárcenas and A. Penlidis, *Macromol. Theory Simul.*, 2008, **17**, 280–289.

20 P. López-Domínguez, G. Jaramillo-Soto and E. Vivaldo-Lima, *Macromol. React. Eng.*, 2018, **12**, 1800011.

21 I. A. Quintero-Ortega, E. Vivaldo-Lima, G. Luna-Bárcenas, J. F. J. Alvarado, J. F. Louvier-Hernández and I. C. Sanchez*, Ind. Eng. Chem. Res.*, 2005, **44**, 2823–2844.

22 I. A. Quintero-Ortega, E. Vivaldo-Lima, R. B. Gupta, G. Luna Bárcenas and A. Penlidis, J. *Macromol. Sci., Part A: Pure Appl. Chem.*, 2007, **44**, 205–213.

23 I. A. Quintero-Ortega, G. Jaramillo-Soto, P. R. García-Morán, M. L. Castellanos-Cárdenas, G. Luna-Bárcenas and E. Vivaldo-Lima, *Macromol. React. Eng.*, 2008, **2**, 304–320.

24 I. A. Quintero-Ortega, P. R. García-Morán, G. Jaramillo-Soto, E. Vivaldo-Lima and G. Luna-Bárcenas, *Macromol. Symp.*, 2009, **283–284**, 103–109.

25 P. López-Domínguez, J. C. Hernández-Ortiz and E. Vivaldo-Lima, *Macromol. Theory Simul.*, 2018, **27**, 1700064.

26  M. Z. Hossain and A. S. Teja, *J. Supercrit. Fluids*, 2015, **96**, 313–323.

27  F. Tumakaka, J. Gross and G. Sadowski, *Fluid Phase Equilib.*, 2005, **228–229**, 89–98.

28  J. Gross and G. Sadowski*, Ind. Eng. Chem. Res.*, 2001, **40**, 1244–1260.

29  J. Gross and G. Sadowski, *Ind. Eng. Chem. Res.*, 2002, **41**, 1084–1093.

30  M. Görnert and G. Sadowski, *J. Supercrit. Fluids*, 2008, **46**, 218–225.

31  P. Vana, T. P. Davis and C. Barner-Kowollik, *Macromol. Theory Simul.*, 2002, **11**, 823–835.

32  N. De Rybel, P. H. M. Van Steenberge, M.-F. Reyniers, C. Barner-Kowollik, D. R. D'hooge and G. B. Marin*, Macromol. Theory Simul.*, 2017, **26**(1), 1600048.

33  G. Jaramillo-Soto, P. R. García-Morán and E. Vivaldo-Lima, *Macromol. Symp.*, 2010, **289**, 149–154.

34  J. Chiefari, Y. K. Chong, F. Ercole, J. Krstina, J. Jeffery, T. P. T. Le, R. T. A. Mayadunne, G. F. Meijs, C. L. Moad, G. Moad, E. Rizzardo and S. H. Thang, *Macromolecules*, 1998, **31**, 5559–5562.

35  J. Pallares, G. Jaramillo-Soto, C. Flores-Cataño, E. Vivaldo-Lima, L. M. F. Lona, A. Penlidis and J. *Macromol, Sci.*, Pure Appl. Chem., 2006, **43**(9), 1293–1322.

36  C. Kiparissides, N. Pagalos, C. Chatzidoukas and C. Mantelis, in *International Conference of High-Pressure Chemical Engineering*, Karlsruhe, Germany, March 3–5, 1999, pp. 27–30.

37  P. B. Zetterlund and S. Perrier, *Macromolecules*, 2011, **44**, 1340–1346.

38  L. Hlalele, R. Pfukwa and B. Klumperman, *Eur. Polym. J.*, 2017, **95**, 596–605.

39  M. Wulkow, M. Busch, T. P. Davis and C. Barner-Kowollik, *J. Polym. Sci., Part A: Polym. Chem.*, 2004, **42**, 1441–1448.

40  P. F. Arce and M. Aznar, *Fluid Phase Equilib.*, 2009, **286**, 17–27.

41  N. von Solms, M. L. Michelsen and G. M. Kontogeorgis, *Ind. Eng. Chem. Res.*, 2003, **42**, 1098–1105.

42 P. López-Domínguez, J. Olvera-Mancilla, J. Palacios-Alquisira, L. Alexandrova, M. A. Dubé and E. Vivaldo-Lima, *J. Macromol. Sci., Part A: Pure Appl. Chem.*, 2018, **55**, 231–242.

43 A. C. Hindmarsh, P. N. Brown, K. E. Grant, S. L. Lee, R. Serban, D. E. Shumaker and C. S. Woodward, *ACM Trans. Math. Softw.*, 2005, **31**, 363–396.

44 Aspen Polymers, *User Guide Volume 2: Physical Property Methods & Models*, Aspen Technology, Inc., Burlington, MA, USA, 2008.

45 Nouryon, Initiator for acrylics manufacturing, https://polymerchemistry.nouryon.com/siteassets/brochures/brochure-initiator-for-acrylics-manufacturing-oct2019.pdf, accessed January 2020).

46 M. Zhang and W. H. Ray, *Ind. Eng. Chem. Res.*, 2001, **40**, 4336–4352.

47 P. López-Domínguez and E. Vivaldo-Lima, *Macromol. React. Eng.*, 2013, **7**, 463–476.

48 N. I. Uzun, M. Akgün, N. Baran, S. Deniz and S. Dinçer, *J. Chem. Eng. Data*, 2005, **50**, 1144–1147.

49 A. Rajendran, B. Bonavoglia, N. Forrer, G. Storti, M. Mazzotti and M. Morbidelli, *Ind. Eng. Chem. Res.*, 2005, **44**, 2549–2560.

50 S. Masoumi, T. A. Duever, A. Penlidis, R. Azimi, P. López-Domínguez and E. Vivaldo-Lima, *Macromol. Theory Simul.*, 2018, 27(5), 1800016.

51 J. C. Hernández-Ortiz, G. Jaramillo-Soto, J. Palacios-Alquisira and E. Vivaldo-Lima, *Macromol. React. Eng.*, 2010, **4**, 210–221.

52 W. Meiser, J. Barth, M. Buback, H. Kattner and P. Vana, *Macromolecules*, 2011, **44**, 2474–2480.

53 M. L. Coote, *J. Phys. Chem. A*, 2005, **109**, 1230–1239.